Experimental Research on Bending Performance of Wood-concrete Composite Slab with Screw Connections

Hao Du,[a] Jiangtao Mei,[b] Weijie Fu,[c] and Xiamin Hu [c,*]

The existing research primarily focuses on wood-concrete composite beams, with limited studies on the bending performance and effective width of wood-concrete composite slabs. A full-scale composite slab with screw connections was constructed and subjected to static load testing. The study extensively investigated the ultimate bearing capacity, load-deflection curves, interface slips, strain distributions of cross-section and effective width of the wood-concrete composite slab. It was found that the failure mechanism of the composite slab involved both bending and tensile failure of the wood beams. As the applied load intensified, a marked augmentation in the longitudinal strain of the concrete slab was observed; along the width direction, the longitudinal strain of concrete slab manifested a curved distribution. The precise determination of the effective width of the concrete slab within the composite floor could be accurately achieved *via* the utilization of a simplified computational approach. In order to simplify the analysis, the M-shaped section of composite slab was approximated as T-section composite beams when evaluating the bending behavior. The linear-elastic model was shown to be accurate in predicting the bending stiffness and load-carrying capacity of composite slabs.

DOI: 10.15376/biores.19.1.1558-1570

Keywords: Wood-concrete composite slab; Bending performance; Bending test; Effective width

Contact information: a: College of Civil Engineering, Nanjing Forestry University, Nanjing 210037, China; b: Construction Eighth Bureau Third Construction Co. LTD, Nanjing 210012, China; c: College of Civil Engineering, Sanjiang University, Nanjing 210012, China;
** Corresponding author: huxm_njtech@163.com*

INTRODUCTION

Wood structures offer several advantages, such as lightweight construction, energy efficiency, environmental sustainability, and aesthetic appeal. With the advent of modern technological advancements, wooden structures have garnered extensive utilization in public constructions, residential buildings, and even towering high-rises (Pastori *et al.* 2022). Within such constructions, the floor is crucial in providing support for vertical loads and furnishing resistance against lateral forces. The wood-concrete composite slab emerges as an innovative variant of the wood slab. It amalgamates wood members and concrete slabs into a cohesive structure through shear connections, thereby facilitating the utilization of the material properties (Yeoh *et al*. 2011a; Chen *et al*. 2023; Du *et al*. 2023). The wood-concrete composite slabs retain the excellent characteristics of wooden floors while enhancing mechanical performance, sound insulation properties, and fire resistance (Deam *et al.* 2008a, b; Zhang *et al.* 2020; Li *et al*. 2023).

Shear connectors play a crucial role in ensuring effective collaboration between wood beams and concrete slabs (Cao *et al*. 2023; Li *et al*. 2023; Yuan *et al*. 2023). Ahmadi and Saka (1993) conducted a study on the shear behavior of screw fasteners with various

shapes and found that increasing the embedded length of screw fasteners in wood beams significantly improved their shearing capacity. Gelfi *et al.* (2002) performed shear experiments on screw connections in the composite beam with interlayer boards and investigated the influence of inter-layer board thickness and screw diameter on the shear performance. The mechanical model for shear stiffness was established based on Winkler's elastic foundation beam theory. Fragiacomo *et al.* (2007) studied the effects of concrete types and concrete strength on the mechanical properties of stud connections. The results indicated that the concrete type had minimal impact on mechanical behavior of stud connections, whereas the shear performance of screw connectors primarily depended on the compressive strength parallel to the wood grain. Deam *et al.* (2008a,b) explored the influence of notch shape, template material and screw type on the shear performance of connectors through push-out tests. The results showed that screw connectors and notched connectors exhibited the best overall performance.

Gelfi *et al*. (1999) discovered that wood floors exhibited excessive deflection deformations under long-term loads, which compromised the functionality. In contrast, wood-concrete composite structures demonstrated significant improvements in bending stiffness and load-bearing capacity. Extensive research has been conducted on wood-concrete composite beams to study failure mechanisms, composite action, and bending performance (Yeoh *et al*. 2011b; Crocetti *et al.* 2015; Du *et al*. 2021). The bending behavior of wood-concrete composite beam is primarily influenced by shear connector type, spacing of shear connections, and section size. The degree of shear connection in composite beam improves with higher slip modulus and closer arrangement spacing of shear connections (Khorsandnia *et al*. 2012; Hong *et al.* 2019). Frangi *et al.* (2003) analyzed the elastic-plastic behavior of the composite beam with ductile connectors and proposed a calculation method for load carrying capacity. It was established that the "γ method" from Eurocode 5 could be utilized within the linear range, and the ductility of shear connectors should be considered in the elastic-plastic analysis of wood-concrete composite beams. Crocetti *et al.* (2015) established a two-dimensional finite element model of wood-concrete beams, integrating the concrete slabs through shell elements and the wood beams simulated by beam elements. The shear connections were modeled as non-linear springs. Subsequent analyses employed three-dimensional finite element models, incorporating solid elements and established stress-strain relationships, to scrutinize the impacts of material properties and the composite action at the interface (Fragiacomo *et al.* 2014). Khai *et al.* (2018) conducted an experimental study on Cross-Laminated Timber (CLT) concrete composite slabs under static and dynamic load conditions. The results revealed that the load-carrying capacity and vibration performance of CLT-concrete composite slabs were significantly improved compared to ordinary CLT floors.

The existing research primarily has focused on the wood-concrete composite beam, with limited studies on the bending performance and effective width of wood-concrete composite slabs. Thus, a full-scale composite slab was constructed and subjected to static load testing. This paper thoroughly investigated ultimate bearing capacity, load-deflection curves, interfacial slippage, strain distributions of cross-section, and effective width of the wood-concrete composite slab. The acquired test outcomes were used to verify the existing calculation method for determining the effective width. Additionally, a simplified calculation model for the composite slab was presented, and the analytical method for determining the bending stiffness and load-carrying capacity composite slabs was substantiated.

EXPERIMENTAL

Wood-concrete Composite Slab Specimen

A full-scale wood-concrete composite slab with screw connectors was constructed and subjected to six-point bending load. The composite slab consisted of four glulam beams, each measuring 4000 mm × 100 mm × 200 mm. The beams were spaced at 967 mm intervals. The concrete slab, which was integrated with the glulam beams, had dimensions of 4000 mm × 3000 mm × 80 mm, as presented in Fig. 1a. To reinforce the concrete slab, steel reinforcement bars of 10 mm diameter were incorporated at intervals of 200 mm within the slab. In the composite slab, lag screw connectors were installed on the top surface of wood beams with a longitudinal spacing of 150 mm, as illustrated in Fig. 1b. The thread diameter and shank diameter of the screw fasteners were 12 mm. The threaded length of the screws was 160 mm. The screw fasteners were fixed with a length of 120 mm into the wood beams and 60 mm into the concrete slab.

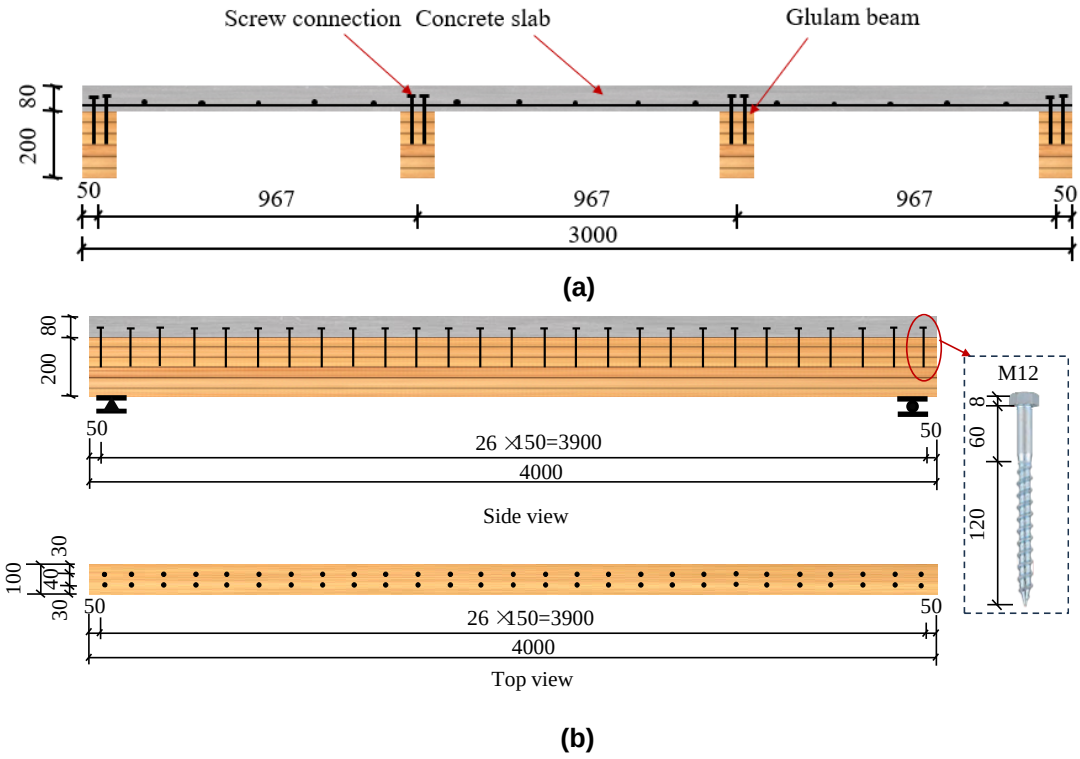

Fig. 1. Details of composite slab specimen: (a) Cross-section of the composite slab; (b) Arrangement of screw connections in the wood beam

Materials

The glulam members used in the composite slab were constructed from larch lumber pieces. The mean density and moisture content of the wood were recorded as 562 kg/m^3 and 14.4%, respectively. To ascertain the mechanical behaviors of the wood components, axial compression tests were conducted on six short column specimens following the guidelines of GB/T 15777 (2012). The mean compressive elasticity modulus was found to be 12570 MPa, and the compression strength oriented parallel to the grain direction was measured at 53.9 MPa. Three cube specimens with dimensions of 150 mm × 150 mm × 150 mm were tested to obtain the concrete compression strength in accordance

with GB/T 50329 (2002). The average axial compression strength of the concrete was 27.3 MPa. The lag screws used in the composite slab exhibited a mean yield strength of 370 MPa and an ultimate tension strength of 463 MPa. The shear strength and slip modulus of one pair of screw fasteners were 40.8 kN and 10.6 kN/mm.

Bending Test Setup

The composite slab was supported as a simply supported beam with a span of 3800 mm. To apply static loading, a hydraulic jack was used along with four-stage distribution beams. The equivalent concentrated loads were administered to emulate uniformly distributed loads across the slab (Fig. 2). The distribution beams were connected with hinged supports to ensure a stable contact surface. The self-weight of the loading devices, jacks and other loading equipment served as the first level load. The composite slab was preloaded to test the loading device and measurement system. The loads were gradually elevated to 5% of the anticipated maximum load at a speed of 0.5 kN/s, followed by a release. Subsequently, the loads were ratcheted up in steps to 90% of the anticipated maximum load, with each step increasing by 25 kN. During this process, crack patterns, strain and deflection data of the composite slab were carefully observed and recorded. Finally, the load was further increased using the displacement control method until the composite slab reached its ultimate limit and was damaged.

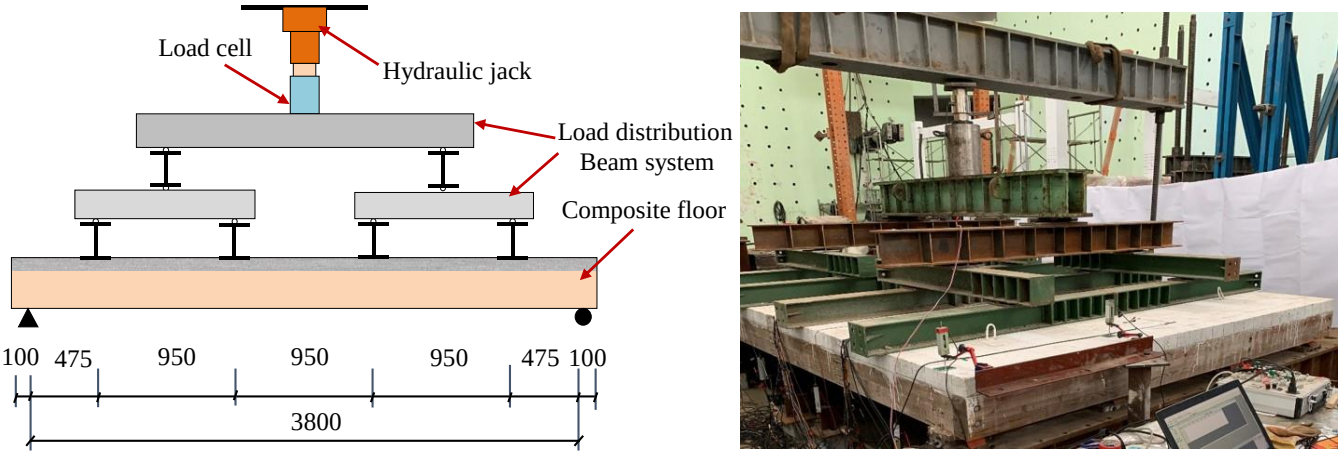

Fig. 2. Bending test of the composite slab

Figure 3 illustrates the configuration of the displacement transducers and foil strain gauges used in the bending test of the composite slab. The placement of these measurement devices was strategically chosen to capture various deformation and strain parameters. The displacement gauge was deployed at the mid-span and loading point of both middle beam and side beam. This allowed for the measurement of displacements at these critical locations under load. Additionally, the displacement gauges were positioned at the supports of the composite slab to obtain settlement displacements, which were used to correct the measured values of mid-span deflection. The strain gauges were arranged at the top surface of the concrete slab in the longitudinal direction to determine the strain distribution and effective width of the concrete slab. To measure the cross-section strain distribution of the wood beams, strain gauge was strategically positioned along the vertical axis at both the mid-span and quarter-span locations of the beams. This enabled the evaluation of strain distribution across the composite cross-section.

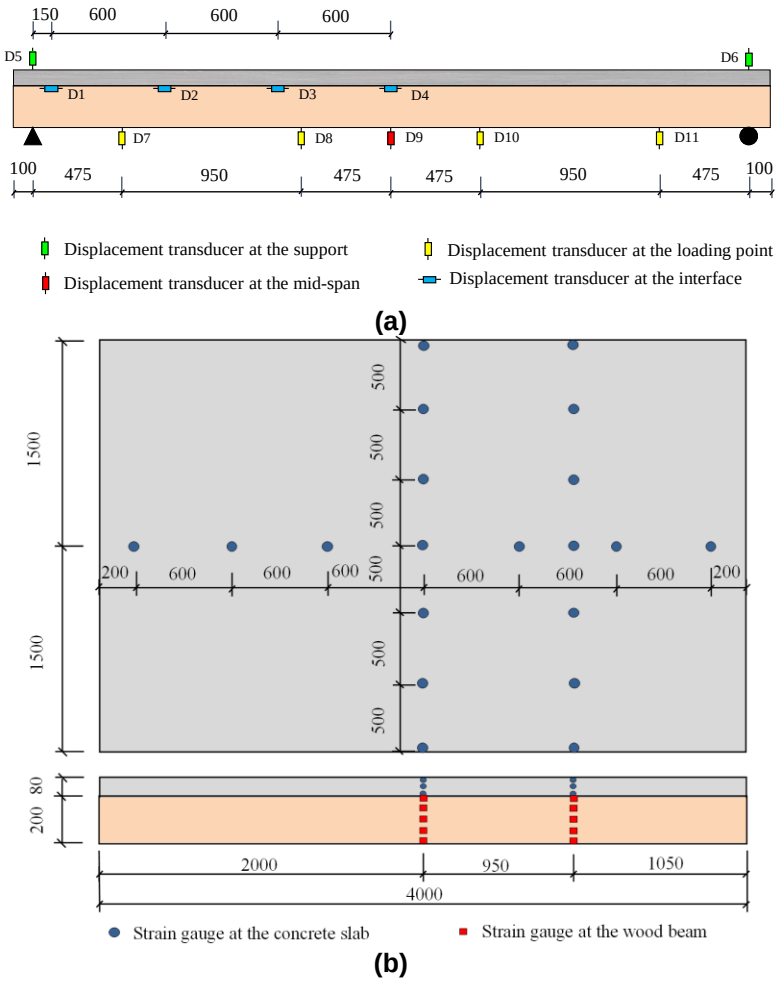

Fig. 3. Configuration of the displacement transducers and foil strain gauges: (a) Arrangement of displacement transducers; (b) Configuration of strain gauges

RESULTS AND DISCUSSION

Bending Behavior and Failure Mechanism

In the early phase of loading, the composite slab demonstrated commendable overall performance, characterized by negligible interfacial slip and lifting displacement between the concrete slab and the wood beams. Nonetheless, with the escalation of the applied loads, some cracks and damage became manifest. When the load reached 190 kN, diagonal cracks appeared in the wood beam at the support position under the shear stresses (Fig. 4a). These cracks resulted from the development of tension stresses. When the load increased to 222 kN, longitudinal cracks were observed along the span direction of the side beam (Fig. 4b). The incidence of transverse cracks within the concrete slab escalated and propagated with the ongoing augmentation of load. Upon reaching a load of 341 kN, a discernible tearing sound emanated, signifying substantial damage to the wood beams. An evident interface separation materialized between the wood members and the concrete slab towards the extremity of the composite slab. When the applied load reached 498.7 kN, a brittle failure occurred in the wood-concrete composite slab. The wood beam experienced tension failure, resulting in a through crack (Fig. 4c). Additionally, transverse cracks were

observed on the side and bottom surfaces of concrete slab (Fig. 4d). These observations indicated that the composite slab underwent progressive damage and ultimately experienced a brittle failure under the applied load. The cracks, separation, and failure observed in both the wood beams and concrete slab indicated the limitations and failure mechanisms of the composite system under significant loading conditions.

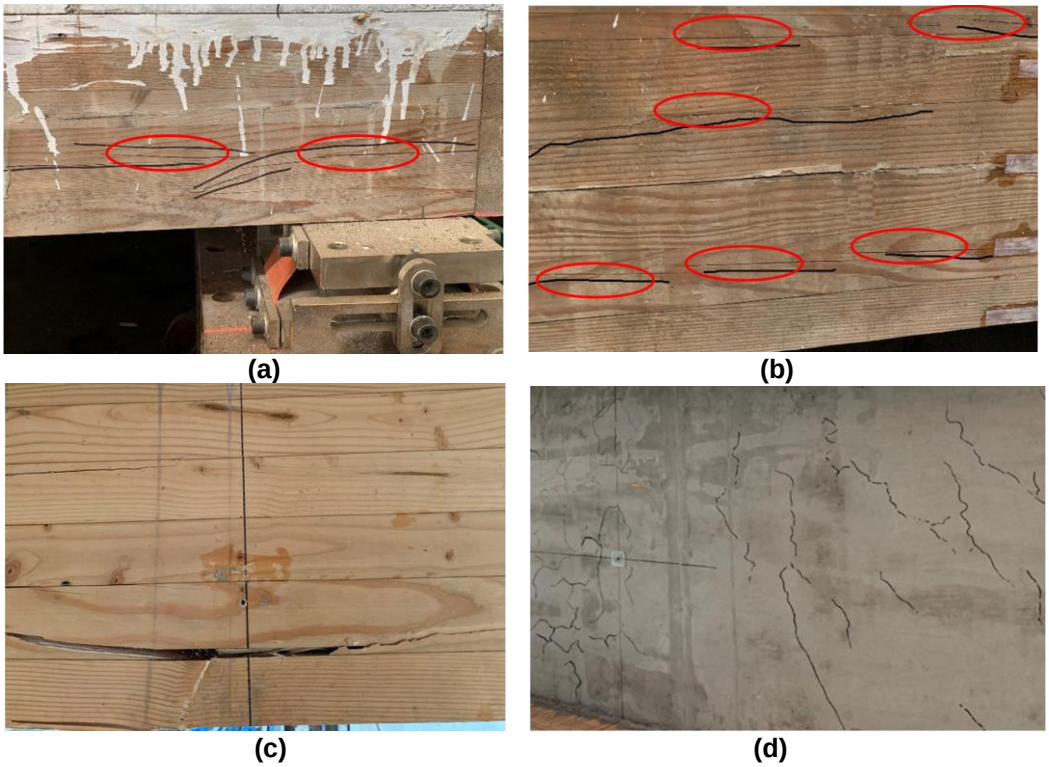

Fig. 4. Test phenomenon and failure mode: (a) Wood cracks at the support; (b) Wood cracks along the span direction; (c) Tensile failure of the wood member; (d) Cracks at the bottom of concrete slab

Load-deflection Behavior

Figure 5 compares the applied load and mid-span deflection observed in the wood-concrete composite slab. In the early stage of loading, the deflection of composite slab increased linearly as the applied load increased. Upon reaching about 72% of the maximum load, the deflection curve transitioned from linearity, manifesting a nonlinear escalation with the increment of applied load. This nonlinear behavior signified a decrement in the bending stiffness of the composite slab. The diminution in bending stiffness was ascribed to pronounced bending deformation endured by the screw connectors under shear forces. The bending deformation resulted in a reduction of the shear stiffness of screw connectors, thereby weakening on the interfacial combination effect. The deflection deformation exhibited by the central beam within the composite slab surpassed that of the lateral beam. This discrepancy in deflection occurred when the central beam shouldered a larger fraction of the applied load compared to the lateral beam. At the ultimate load, a sharp reduction in load occurred due to the brittle failure of the wood beam, accompanied by a rise in deflection. Overall, the deflection behavior of the wood-concrete composite slab indicated a gradual reduction in bending stiffness as the load increased and ultimately experienced brittle failure of the wood beam, leading to a sharp decrease in load-carrying capacity.

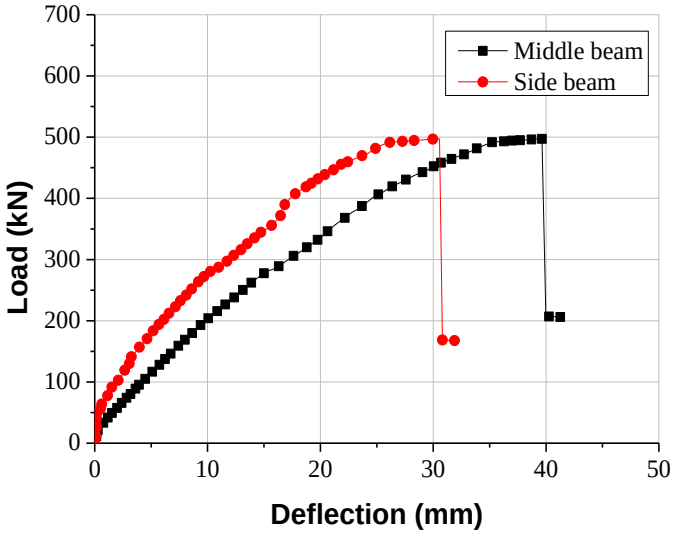

Fig. 5. Load-deflection curve of wood-concrete composite slab

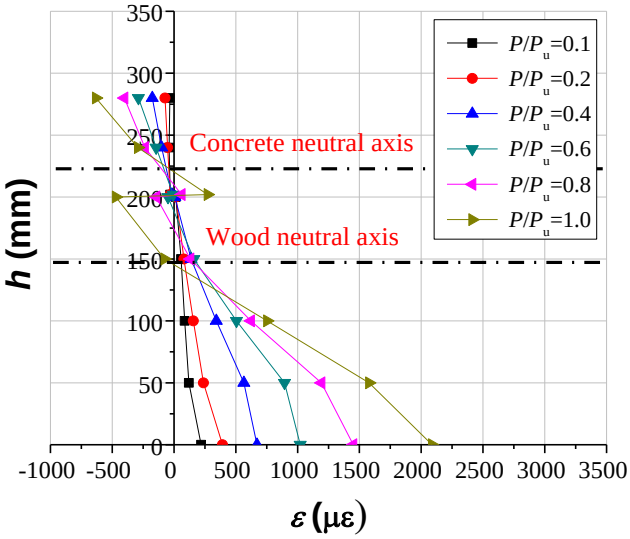

Fig. 6. Strain distributions of composite section at the mid-span

Strain Distribution of Composite Slab

Figure 6 displays the strain distribution of composite section at the mid-span. During the early loading phase, the cross-section strain distribution approximated a linear pattern. This indicated that the assumption of plane section was satisfied. The wood beams and concrete slab bore the bending loads and produced coordinate deformation together. As the load increased, the cross-section strain distribution deviated from plane section assumption. This deviation was primarily caused by the interfacial slips between wood beam and concrete slab. The interfacial slips resulted in changes in the neutral axis positions of both components. The neutral axis within wood member experienced a descending shift towards the beam center, while the neutral axis within concrete slab exhibited an ascending movement towards the slab's center. As a consequence of these changes in neutral axis positions, the strain distribution within the composite section became discontinuous and less uniform (Tao *et al.* 2022). The discontinuity in strain distribution became increasingly pronounced with the increase of load. Collectively, the strain distribution analysis illuminated the impact of relative slips between the wood beam and concrete slab on the mechanical behavior of the composite slab. Initially, the assumption of a plane section was satisfied. However, it was invalidated with the escalating load, engendering notable alterations in the strain distributions and positions of neutral axes within composite components.

Figure 7 displays the strain distributions within concrete slab across the width direction. During the initial loading phase, the longitudinal strains of concrete slab exhibited consistent distributions across the width. This indicated that the concrete slab was initially under relatively uniform stress. With the increase of the applied load, a marked augmentation in the longitudinal strain of the concrete slab was observed, chiefly attributable to the concrete cracking. The longitudinal strains within the concrete slab displayed curved distributions across the width. This uneven distribution emanated from the shear deformations and shear lag effects inherent in the concrete slab. These phenomena rendered the strains more pronounced at the mid-span of the concrete slab in comparison to the quarter-span locations. In summary, the strain distribution analysis of

the concrete slab revealed the development of cracks and the influence of shear deformation and shear lag effect. The strain distributions initially manifested uniformity but transitioned to a curved profile across the slab width as the load increased. These observations offered insights into the comportment of the concrete slab under loading conditions and underscore the uneven stress distribution engendered by the shear lag effect.

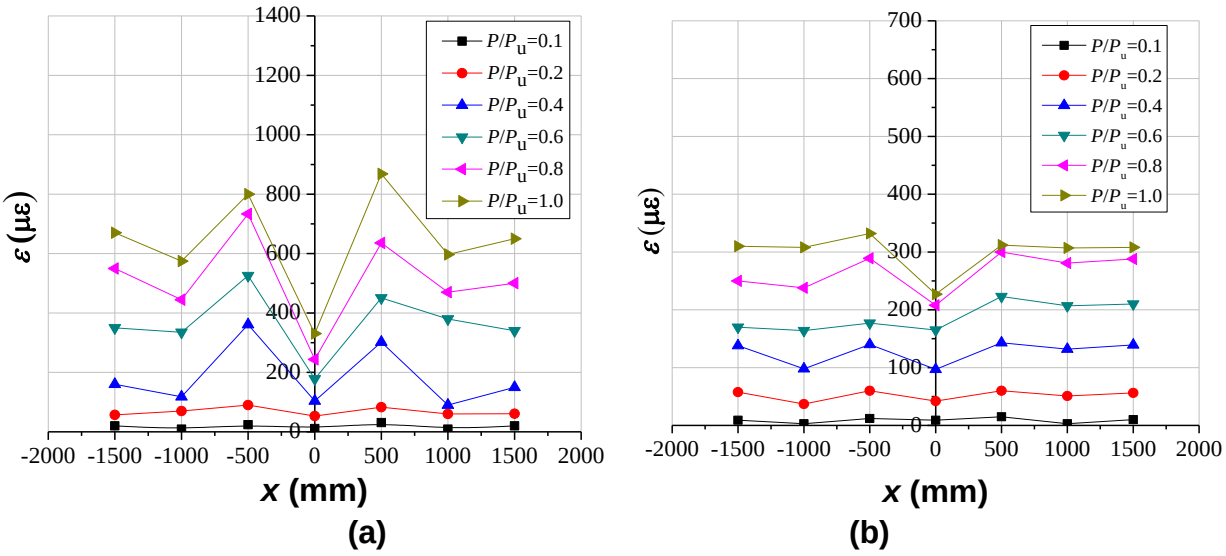

Fig. 7. Strain distributions of concrete slab at (a) mid-span and (b) quarter-span

Bending Stiffness of Composite Slab

The compressive stress of concrete slab in the composite slab was uniformly distributed along the width direction. The main reason was that the shear deformation and shear lag effect occurred in concrete slab. To consider the effect of non-uniform distributions of compressive stress within concretes slab, the effective width of the concrete slab b_{eff} was employed. It was postulated that the compressive stresses exhibited a uniform distribution within the span of the effective width, and the compressive stresses of concrete outside the effective width were not considered. To predict the bending stiffness of composite slab, the effective width of the concrete slab had to be ascertained. The simplified calculation method for the effective width of concrete slab in T-section bending member was presented in GB 50010 (2010),

$$b_{\text{eff}} = \min \begin{cases} b_{\text{t}} + 12h_{\text{c}} \\ b_{\text{t}} + s_{\text{n}} \\ l_0 / 3 \end{cases} \quad (1)$$

where b_t is wood beam width, h_c is concrete slab thickness, s_n is clear distance between rib beam, and l_0 is beam span.

The M-shaped cross-section of the composite slab is derived to a T-section composite beam (Fig. 8). The wood-concrete composite slab using ductile connections can be considered as a floor system exhibiting partial composite action. When subjected to bending loads, there are relative slips at the wood-concrete interface. Therefore, the influence of interface slips needs to be considered in calculating the bending stiffness. Presently, the linear-elastic analytical model is prevalently employed in the design of wood-concrete composite beams integrated using ductile connections. This model assumed

that all constituent materials (concrete, wood, and shear connections) persist in the linear elastic stage until the wood members were destroyed. Eurocode 5 (2004) provides a simplified computational approach to ascertain the bending stiffness of the beams with partial composite action. By using this analytical model, the bending stiffness of wood-concrete composite slab could be estimated, considering the impact of interfacial slips and the linear-elastic behavior of the composite components involved. This allows for a more accurate prediction of the structural response and performance of the composite slab during bending.

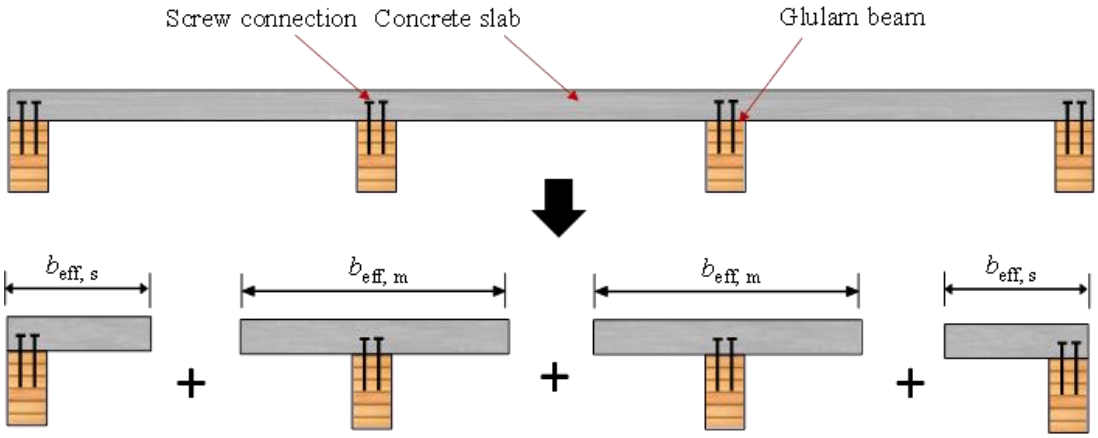

Fig. 8. Calculation model of T-section composite beam

$$EI_{\text{eff}} = E_1 I_1 + E_2 I_2 + \gamma_1 E_1 A_1 a_1^2 + \gamma_2 E_2 A_2 a_2^2 \quad (2)$$

$$\gamma_1 = \frac{1}{1 + \frac{\pi^2 E_1 A_1 s}{KL^2}} \quad (3)$$

$$a_2 = \frac{\gamma_1 E_1 A_1 (h_1/2 + h_2/2)}{\gamma_1 E_1 A_1 + \gamma_2 E_2 A_2} \quad (4)$$

$$a_1 = \frac{h_1 + h_2}{2} - a_2 \quad (5)$$

In Eqs. 2 through 5, EI_{eff} is bending stiffness of composite beams, K is service slip modulus of screw connection, s is spacing of the shear connector, and L is span of beam.

Bending Capacity of Composite Slab

The linear-elastic analytical model is widely adopted in predicting the bending capacity of wood-concrete composite beam. This approach assumes that the concrete, wood and shear connections remain within the linear elastic range. Consequently, the bending bearing capacity of composite beams was determined according to the ultimate limit state of the timber member, concrete slab and shear connectors. Upon the determination of the bending stiffness EI, the following equations were used to calculate the normal stresses of the timber member and concrete slab:

$$\text{Bending stress: } \sigma_{1,M}(x) = \pm M_i(x)\frac{h_1 E_1}{2EI};\ \sigma_{2,M}(x) = \pm M_i(x)\frac{h_2 E_2}{2EI} \quad (6)$$

$$\text{Axial stress: } \sigma_{1,N}(x) = -M_i(x)\frac{E_1\gamma_1 a_1}{EI};\ \sigma_{2,N}(x) = M_i(x)\frac{E_2\gamma_2 a_2}{EI} \quad (7)$$

The ultimate limit states of the concrete slab and timber member under combined bending and compressive stresses were checked as shown in Eqs. 8 and 9, respectively:

$$\sigma_{1,M}(x) + \sigma_{1,N}(x) \le f_c \quad (8)$$

$$\frac{\sigma_{2,M}(x)}{f_m} + \frac{\sigma_{2,N}(x)}{f_t} \le 1.0 \quad (9)$$

The ultimate limit state of shear connections was checked as:

$$T(x) = \frac{\gamma_1 E_1 A_1 a_1 s(x)}{EI} V(x) \le T_R \quad (10)$$

where f_c is compression strength of concrete, f_m is bending strength of wood, f_t is tensile strength of wood, and T_R is shearing strength of shear connections.

Comparison between Experimental Results and Predicted Results

Table 1 illustrates the specific values of the mid-span deflection and bending capacity for different composite slab specimens, along with the corresponding calculated results. The agreement between the predicted and tested deflection deformations indicated that the calculated bending stiffness of the composite slabs was reliable. Similarly, the comparison of the experimental and predicted bending capacities showed that the analytical method could effectively estimate the ultimate load-carrying capacity of the composite slabs. It could be concluded that the theoretical method adopted for ascertaining the bending stiffness and capacity of wood-concrete composite slabs was valid, yielding precise estimations.

Table 1. Comparison between the Test and Calculated Results

Authors	Specimens	Mid-span Deflection		Δ_t/Δ_c	Bending Capacity		M_t/M_c
		Δ_t (mm)	Δ_c (mm)		M_t (kN·m)	M_c (kN·m)	
This paper	GCCF	15.0	15.9	0.94	42.9	44.7	0.96
Hong *et al*. (2019)	WCCB-1	12.0	11.5	1.04	43.3	32.7	1.32
	WCCB-2	12.0	10.7	1.12	49.5	44.2	1.12
	WCCB-3	12.0	11.2	1.07	46.6	44.2	1.05
	WCCB-4	12.0	10.2	1.18	51.7	58.7	0.88
Frangi *et al*. (2003)	Screws	22.4	21.3	1.05	34.4	33.7	1.02
	Nail plates	22.4	20.6	1.09	39.6	33.6	1.18
	Notches	22.4	22.8	0.98	54.9	47.5	1.16
	Means			1.10			1.09
	Coefficient of Variation (%)			5.1			14.5

Note: Δ_t is experimental result of mid-span deformation at serviceability limit state, Δ_c is predicted result of mid-span deformation under serviceability limit state, M_t is test result of bending capacity, and M_c is calculated result of bending capacity.

CONCLUSIONS

1. In the initial phase of loading, the wood-concrete composite slab demonstrated commendable overall performance, characterized by negligible interfacial slip and lifting displacement between the concrete slab and the wood beams. With the augmentation of load, diagonal cracks in the wood beams at the support position and longitudinal cracks along the span direction of the side beam were observed. Transverse cracks in the concrete slab increased and further developed. At the ultimate load, a brittle failure occurred in the wood beam, leading to a through crack. Transverse cracks were also observed on the side and bottom of concrete slab.
2. The load-deflection behavior showed that the deflection of composite slab initially increased linearly but became nonlinear at approximately 72% of the maximum load. This nonlinearity indicated a reduction in bending stiffness due to large bending deformations in the screw connections and a decrease in shear stiffness and composite action.
3. The analysis of strain distribution elucidated that during the initial loading stage, the strain dispersion across the composite section adhered to the assumption of a plane section. As the load increased, the cross-section strain distribution deviated from plane section assumption. This deviation was primarily caused by the interface slips between wood beam and concrete slab. The interfacial slips resulted in changes in the neutral axis positions of both components.
4. The strain distribution analysis of the concrete slab revealed the development of cracks and the influence of shear deformation and shear lag effect. The strain distributions initially manifested uniformity but transitioned to a curved profile across the slab width as the load increased.
5. The M-shaped cross-section of the composite slab was derived to a T-section composite beam. The theoretical method adopted for ascertaining the bending stiffness and bearing capacity of wood-concrete composite slabs proved to be valid, yielding precise estimations.

ACKNOWLEDGMENTS

The research was supported by National Natural Science Foundation of China (No. 52208257), Natural Science Foundation of Colleges and Universities of Jiangsu Province (22KJB560023), and China Postdoctoral Science Foundation (2023M731711).

REFERENCES CITED

Ahmadi, B.H., and Saka, M.P. (1993). "Behavior of composite timber-concrete floors," *Journal of Structural Engineering* 119(11), 3111-3130. DOI: 10.1061/(ASCE)0733-9445(1993)119:11(3111)

Cao, Q., Wei, Y., Chen, S., Lin, Y., and Ding, M. (2023). "Experimental investigations on the load-bearing properties of dowel connection joints of bamboo scrimber," *Structures* 50, 1868-1878. DOI: 10.1016/j.istruc.2023.03.022

Chen, S., Wei, Y., Wang, G., Zhao, K., and Ding, M. (2023). "Mechanical behavior of laminated bamboo-timber composite columns under axial compression," *Archives of Civil and Mechanical Engineering* 23, 1-12. DOI: 10.1007/s43452-023-00612-y

Crocetti, R., Sartori, T., and Tomasi R. (2015). "Innovative timber-concrete composite structures with prefabricated FRC slabs," *Journal of Structural Engineering* 141(9), article 04014224. DOI: 10.1061/(ASCE)ST.1943-541X.0001203

Deam, B. L., Fragiacomo, M., and Buchanan, A. H. (2008a). "Connections for composite concrete slab and LVL flooring systems," *Materials and Structures* 41(3), 495-507. DOI: 10.1617/s11527-007-9261-x

Deam, B. L., Fragiacomo, M., and Gross, L. S. (2008b). "Experimental behavior of prestressed LVL-concrete composite beams," *Journal of Structural Engineering* 134(5), 801-809. DOI: 10.1061/(ASCE)0733-9445(2008)134:5(801)

Du, H., Hu, X., Meng, Y., and Xie, Z. (2023). "Study of the shear performance of inclined screws in glulam-concrete composite beams under standard ISO 834 fire," *Fire Safety Journal* 141, 103975. DOI: 10.1016/j.firesaf.2023.103975

Du, H., Hu, X., Xie, Z., and Meng, Y. (2021). "Experimental and analytical investigation on fire resistance of glulam-concrete composite beams," *Journal of Building Engineering* 44, 103244. DOI: 10.1016/j.jobe.2021.103244

Du, H., Liu, J., Yuan, S., Shi, D., and Hu, X. (2023). "Mechanical behavior of glulam-concrete composite beam with notched connections under ISO 834 standard fire," *Journal of Building Engineering* 78, article 107670. DOI: 10.1016/j.jobe.2023.107670

EN 1995-1-1: 2004, Eurocode 5 (2004). "Design of timber structures – Part 1-1: General rules and rules for buildings," European Committee for Standardization, Brussels, Belgium.

Fragiacomo, M., Amadio, C., and Macorini, L. (2007). "Short- and long-term performance of the Tecnaria stud connector for timber-concrete composite beams," *Materials and Structures* 40(10), 1013-1026. DOI: 10.1617/s11527-006-9200-2

Fragiacomo, M., Balogh, J., To, L., and Gutkowski, R. M. (2014). "Three-dimensional modeling of long-term structural behavior of wood-concrete composite beams," *Journal of Structural Engineering* 140 (8), article A4014006. DOI: 10.1061/(ASCE)ST.1943-541X.0000909

Frangi, A., and Fontana, M. (2003). "Elastoplastic model for timber-concrete composite beams with ductile connection," *Structural Engineering International* 13(1), 47-57. DOI: 10.2749/101686603777964856

GB/T 15777 (2017). "Method for determination of the modulus of elasticity in compression parallel to grain of wood," Standards Press of China, China.

GB/T 50010 (2010). "Code for design of concrete structures," Standards Press of China, China.

GB/T 50081 (2002). "Standard for test methods of mechanical properties on ordinary concrete," Standards Press of China, China.

Gelfi, P., and Giuriani, E. (1999). "Stud shear connectors in wood-concrete composite beams," in: *Proceedings of the first international RILEM symposium on timber engineering*, Stockholm, Sweden, pp. 13-15.

Gelfi, P., Giuriani, E., and Marini, A. (2002). "Stud shear connection design for composite concrete slab and wood beams," *Journal of Structural Engineering* 128(12), 1544-1551. DOI: 10.1061/(ASCE)0733-9445(2002)128:12(1544)

Hong, W., Jiang, Y., Fang, Y., and Hu, X. (2019). "Experimental study and theoretical

analysis of glulam-concrete composite beams connected with ductile shear connectors," *Advances in Structural Engineering* 23(6), 1168-1178. DOI: 10.1177/1369433219891560

Khai, Q. M., Aron, P., Khoa, T. N., and Lee, K. (2018). "Full-scale static and dynamic experiments of hybrid CLT-concrete composite slab," *Construction and Building Materials* 170, 55-65. DOI: 10.1016/j.conbuildmat.2018.03.042

Khorsandnia, N., Valipour, H. R., and Crews, K. (2012). "Experimental and analytical investigation of short-term behaviour of LVL-concrete composite connections and beams," *Construction and Building Materials* 37(12), 229-238. DOI: 10.1016/j.conbuildmat.2012.07.022

Li, H., Wei, Y., Yan, L., Semple, K. E., and Dai, C. (2023). "Structural behavior of steel dowel strengthened cross-laminated bamboo and timber beams," *Composite Structures* 318, article 117111. DOI: 10.1016/j.compstruct.2023.117111

Pastori, S., Mazzucchelli, E. S., and Wallhagen, M. (2022). "Hybrid timber-based structures: A state of the art review," *Construction and Building Materials* 359, article 129505. DOI: 10.1016/j.conbuildmat.2022.129505

Tao, H., Yang, H., Ju, G., Xu, J., and Shi, B. (2022). "Effective width of timber-concrete composite beams with crossed inclined coach screw connections at the serviceability state," *Engineering structures* 267, article 114716. DOI: 10.1016/j.engstruct.2022.114716

Yeoh, D., Fragiacomo, M., Franceschi, M. D., and Boon, K. H. (2011a). "State of the art on timber-concrete composite structures: Literature review," *Journal of Structural Engineering* 137(10), 1085-1095. DOI: 10.1061/(ASCE)ST.1943-541X.0000353

Yeoh, D., Fragiacomo, M., and Deam, B. (2011b). "Experimental behaviour of LVL-concrete composite slab beams at strength limit state," *Engineering Structures* 33, 2697-2707. DOI: 10.1016/j.engstruct.2011.05.021

Yuan, S., Du, H., Sun, Z., and Hu, X. (2023). "Experimental and numerical study on shear performance of pitched screws in wood-concrete composite beam with wooden partitions," *Materials* 16, article 5098. DOI: 10.3390/ma16145098

Zhang, X., Hu, X., Gong, H., Zhang, J., Lv, Z., and Hong, W. (2020). "Experimental study on the impact sound insulation of cross laminated timber and timber-concrete composite floors," *Applied Acoustics* 161, article 107173. DOI: 10.1016/j.apacoust.2019.107173

Article submitted: December 11, 2023; Peer review completed: January 3, 2024; Revised version received: January 9, 2024; Accepted: January 12, 2024; Published: January 19, 2024.
DOI: 10.15376/biores.19.1.1558-1570